ACS APPLIED MATERIALS & INTERFACES

Research Article

www.acsami.org

Embedded Surface Relief Gratings by a Simple Method to Improve Absorption and Electrical Properties of Polymer Solar Cells

Kan Li, Hongyu Zhen,* Zhuoyin Huang, Guolong Li, and Xu Liu

State Key Laboratory of Modern Optical Instrumentation, Zhejiang University, Hangzhou 310027, China

ABSTRACT: We demonstrate a simple rubbing hole injection layer (HIL) to form surface relief gratings (SRGs) on the functional layers of polymer solar cells (PSCs). PSCs studied in this work consist of an ITO/PEDOT:PSS(HIL)/P3HT:PCBM(photoactive layer)/LiF/Al structure. SRGs are successfully formed on HIL in an effective rubbing process, and are over printed on the photoactive layer and cathode consequently. These triplet SRGs change the morphologies of interfaces of PSCs, which can increase optical path lengths, interaction between HIL and P3HT chains, and interface areas between electrode and photoactive layer. Both light trapping and electrical improvement are confirmed by theory and experiments, which lead to overall increase in short-circuit current density, fill factor, and power conversion efficiency (PCE) of PSCs. An average PCE of 3.8% is achieved from PSCs with SRGs without thermal annealing. Different from the directly rubbing the donor polymer film, a suitable degree of orientation of P3HT presents a lower dichroic ratio and higher photovoltaic response in our work.

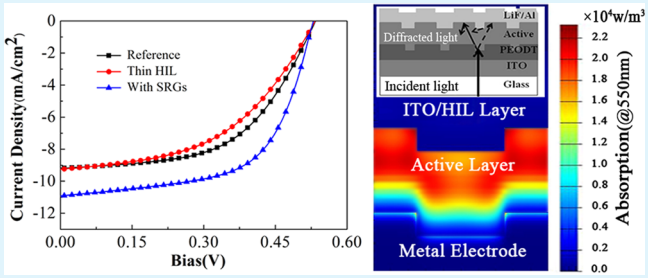

KEYWORDS: *polymer solar cell, surface relief grating, optical path length, interface area, electrical improvement, hole mobility*

1. INTRODUCTION

Polymer solar cells (PSCs) have received considerable attention as attractive alternatives to silicon-based photovoltaic technology due to their unique advantages of low cost, lightweight, and potential application in flexible large-area devices. The bulk heterojunction (BHJ) structure based on phase-separated blends of polymer semiconductors and fullerene derivatives have become one of the most successful device structures developed in the field of organic photovoltaic to date.[1] BHJ has been demonstrated to improve power conversion efficiencies (PCE) by increasing the interface areas between the electron donor and electron acceptor through spontaneous phase separation, which can be obtained using various solution coating technologies.[2,3] In the past decade, several effective methods have been developed to optimize the BHJ, including solvent annealing, thermal annealing, or additives in the solution of donor/acceptor blends.[4−7] On the other hand, because of the low carrier mobility limiting the thickness of photoactive layer, it is still a hot topic on improving light absorption of PSCs. Light trapping schemes such as diffraction gratings, optical spacer layers and folded substrates have been explored in PSCs where improvements are noted.[8,9] Periodic gratings are first used in silicon solar cells and then widely used in PSCs[10] which are formed by soft lithography both at photoactive and hole injection layer (HIL).[11,12] Metallic gratings or nanoparticles including Ag, Au, or other materials have been introduced into PSCs as well.[13−18] Recently, significant progress has been reported in 2D-dot nanopatterned anode of PSCs.[19] Although these works have been impressive, there are still lots of space for the extensive investigation as it is difficult to optimize the absorption and carrier transport simultaneously from optical microstructure in the PSCs. Some work makes great contribution to light absorption, but the device performance has not been enhanced obviously.

Here we demonstrate a simple method to fabricate PSCs with surface relief gratings (SRGs) on all functional layers except for ITO anode. The SRGs are successfully formed on the HIL in an effective rubbing process, and then overprinted on photoactive layer and cathode consequently. Unlike the soft lithography, rubbing process does not decrease the surface energy of the HIL, which will cause difficult film formation of photoactive layer.[20] Furthermore, SRGs formed by rubbing are more convenient to be fabricated. Rubbing technologies are widely used in polarized polymer light emitting devices (PLED),[21] but there are few reported on the rubbing PSCs because of the circularly polarized characteristic of sun light. For the potential application into LCD, PSCs with high dichroic ratio are reported by D. Fichou[22] and Y. Yang.[23] In this work, PSCs with low dichroic ratio and high PCE are achieved without thermal annealing process for BHJ, which demonstrates that SRGs in the functional layers of PSCs can induce higher absorption and electrical improvement.

2. EXPERIMENTAL SECTION

poly(3-hexylthiophene) (P3HT) was obtained from Nichem Fine Technology Co. Ltd. and [6,6]-phenyl-C_{61}-butyric acid

Received: June 12, 2012
Accepted: July 9, 2012
Published: July 9, 2012

   dx.doi.org/10.1021/am301059j | ACS Appl. Mater. Interfaces 2012, 4, 4393−4397

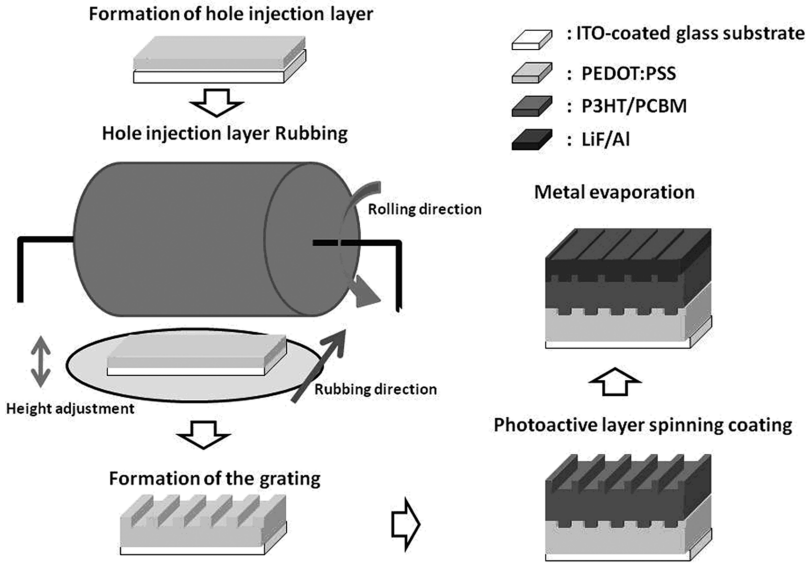

Figure 1. Fabrication process of the PSCs with SRGs in functional layers.

methyl ester (PCBM) was purchased from Flexible Electronics Materials. Both materials were used without further purification. poly(3,4-ethylenedioxythiophene):poly(4-styrene sulfonate) (PEDOT:PSS) was obtained from Bayer AG and diluted with deionized water. A solution of a 1:0.8 weight ratio of P3HT:PCBM in 1,2-dichlorobenzene with a concentration of 25 mg/mL was used. 1, 8-Octanedithiol obtained form Sigma-Aldrich was also added in this solution with a concentration of 25 mg/mL to improve the interpenetrating network morphology of BHJ.[6] The mixture was then stirred for 8 h before spin-coating.

A laboratory-made rubbing device was used to inscribe the SRGs, which consisted of two integral components: an electric-driven roller covered with chosen velvet and a two-dimensional mobile platform. Both speeds of the platform and the roller were adjustable. The SRGs were fabricated at the different rubbing strength (RS) of the rubbing device.[24,25]

The fabrication process and device scheme of the PSCs with SRGs are shown in Figure 1. ITO-coating glass substrates (15Ω/□) were cleaned with detergent, deionized water, acetone, and isopropyl alcohol orderly and then exposed to oxygen plasma for 20 min prior to any deposition. PEDOT: PSS was spin-coated at 2000 rpm on the substrates and annealed at 120^{oC} for 1 h in vacuum, resulting in a thickness of around 50 nm. Then the PEDOT: PSS layer (used as HIL of PSCs) was rubbed by the rubbing device. Later, P3HT:PCBM layer served as photoactive layer was formed by spin-coating from the dichlorobenzene solution at a speed of 1200 rpm for 30 s on the top of rubbed alignment layer. Finally lithium fluoride (0.7 nm) and aluminum (120 nm) as the cathode were deposited by thermal evaporation onto the P3HT:PCBM layer in a vacuum under 8×10^{-4} Pa. The unrubbed PSCs with the same thick HIL (~50 nm) as the rubbed device are studied as reference PSCs and the unrubbed PSCs with thinner HIL (30–40 nm) are also studied. The thicknesses for all the photoactive layers of PSCs are around 100 nm, which are confirmed by surface profilometer. To fabricate the hole-only devices, the molybdenum oxide (50 nm) and Al (100 nm) were evaporated as the top electrode instead of the LiF/Al in the normal devices (the structure of the hole-only devices is ITO/PEDOT:PSS/P3HT:PCBM/MoO_3/Al). Meanwhile, samples with P3HT:PCBM spin-coated on the rubbed and flat HIL were prepared on glass substrate for the absorption measurement.

The scanning electron microscope (SEM) of Ultra 55 Carl Zeiss was used to characterize the morphology of the layers. The details of SRGs were measured by Atomic force microscopy (AFM) (SP13800N Seiko). Absorption spectra were obtained from UV 3101PC spectrometer. The device performances were measured under 100 mW cm^{-2} illumination from a 450W Oriel solar 3A simulator with an AM 1.5G filter in the air. The thicknesses of photoactive layer and HIL were characterized by Dektak 3M surface profilometer.

3. RESULTS AND DISCUSSION

The grating period and depth are determined by the velvet and rubbing strength (*RS*), which is defined as the follows

$$RS = NM\left[\frac{2\pi rn}{60v} - 1\right] \quad (1)$$

Where N is the number of rubbing, M is the contact depth between the HIL and the roller. r and n are the radius and the rotational speed of the roller respectively, and v is the speed of mobile platform. Based on a great amount of experiments, the parameters were chosen as bellows: $N = 1$, $r = 30$ mm, $n \approx 500$ r/min, $v \approx 10$ mm/s, only using different M to change the *RS*. In this work, M was chosen as 0.06 mm with the corresponding *RS* of 10 mm. To study the grating parameters of SRGs fabricated above, the morphologies of the HILs with SRGs are imaged with SEM and AFM, which are shown in images a and b in Figure 2, respectively. The SRGs formed in HILs have an average grating period of around 500 nm and grating depth of 30 nm, which are shown from both images. Stalactite structures were shown on the surfaces of both the grooves and ridges where the surface roughness will be larger. As a result, the incident light could be further bent when it passes through the SRGs. Consequently, the optical path length increases and there are much more opportunities for the light to obtain a total reflection in the rear interface.

Because only the lights absorbed by the photoactive layer contribute to photovoltaic conversion, absorption of photoactive layer is studied based on the optical simulation and test.

dx.doi.org/10.1021/am301059j | ACS Appl. Mater. Interfaces 2012, 4, 4393–4397

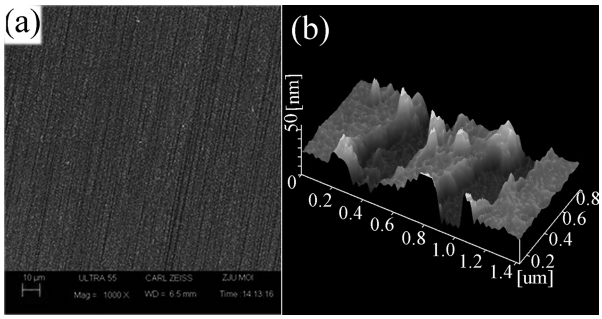

Figure 2. (a) SEM image of HIL with SRGs; (b) AFM image of HIL with SRGs.

With the grating parameters obtained from SEM and AFM images, FDTD method is used in the simulation. Here all the optical constants of the four functional layers: ITO, HIL, photoactive layer, and Al are obtained by a transmission curves fitting method.[26] The PSCs with SRGs in functional layers present obviously higher absorption than the reference PSCs, as shown in Figure 3a. With standard sun light condition (AM 1.5) taken into the calculation, the total photons absorbed by the cells are calculated according to the formulation 2.

$$N_{\text{photon}} = \int_{400}^{700} \frac{\lambda E(\lambda)\text{abs}(\lambda)}{h} d\lambda \quad (2)$$

Here, N_{photon} is the number of absorbed photons; λ is the photon wavelength; $E(\lambda)$ is the energy density of AM1.5 spectrum at wavelength λ; abs(λ) is the absorptance of photoactive layer at wavelength λ; h is the Planck constant. The absorbed photons per square meter of the PSCs with SRGs and the reference PSCs are 7.61×10^{20} and 6.74×10^{20} respectively, 12.9% increase of absorption is attributed to the light trapping effect of SRGs in functional layers.

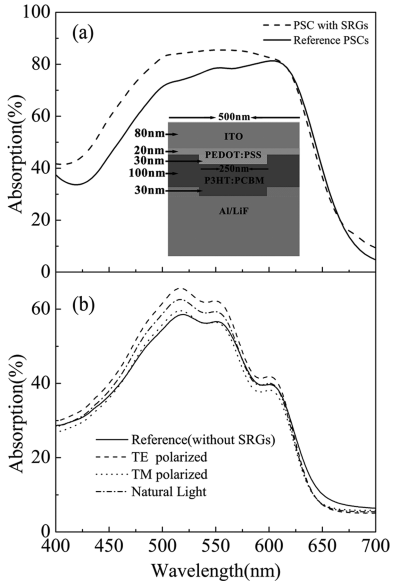

Figure 3. (a) The simulated absorption spectra of PSCs with SRGs and reference PSCs. Inset: the geometrical parameters for the simulation. (b) Absorption spectra of samples in TM polarized (dot line), TE polarized (dash line), natural lights (dash dot line), and the reference sample (without SRGs) (solid line).

Because it is difficult to obtain the absorption spectrum with Al layer, absorption of photoactive layers is tested based on samples with P3HT:PCBM spin-coated on the rubbed and flat HIL. At the same time, the dichroic characteristics of the photoactive layer are also studied. The absorption spectra of samples are recorded on polarized light and natural light from 400 to 700 nm (Figure 3b). When the polarization of incident is perpendicular to the direction of gratings (TE polarized), the sample with SRGs shows a higher absorption compared to the reference (without SRGs), and when the polarization of incident is parallel to the direction of gratings (TM polarized), the absorption is almost the same as the reference (without SRGs). Compared with the directly rubbing donor polymers at high temperature,[23] a lower dichroic ratio is shown by the rubbing HIL without annealing which can prevent the photoactive layer from mechanical damage. But for natural light, their superior absorption to the reference sample demonstrated the light-trapping ability of SRGs. Without the reabsorption from the reflection of Al and the interference from ITO layer, there is some deflection between Figure 3a and Figure 3b, whereas both the enhanced absorption from simulation and test demonstrate light trapping effect of SRGs in functional layers of PSCs.

During the film formation by spin-coating, SRGs with stalactite structure in HIL can lead the orientation of P3HT chains at certain degree, which is confirmed by the polarized absorption of photoactive layer (Figure 3a), a low dichroic ratio shows a low orientation on the plane. Simultaneously, there are lots of irregular protrusions in SRGs formed by rubbing which lead the orientation of P3HT chains in the direction of electrical field. This orientation effect could contribute to the higher mobility. The hole mobility of the PSCs with and without SRGs is studied based on hole-only devices. These devices with electrodes that can suppress injection of electron

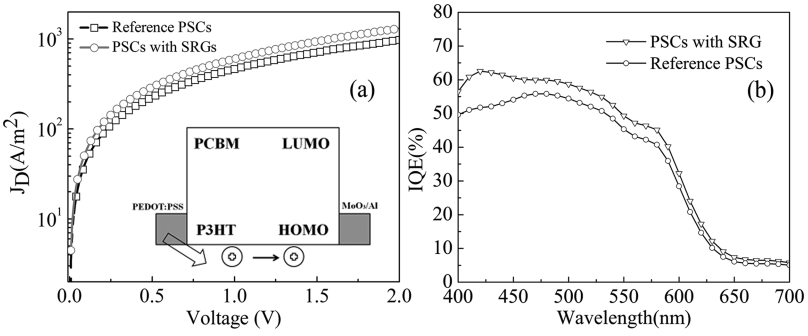

Figure 4. (a) Experimental dark $J-V$ characteristics of PSCs with SRGs and the reference PSCs. Insert: the structure of hole-only devices. (b) The internal quantum efficiency (IQE) of PSCs with SRGs and the reference PSCs.

are characterized with current−voltage (J−V) measurement. An Ohmic contact is formed between PEDOT:PSS and P3HT for hole injection. On the other hand, MoO_3 can strongly suppress electron injection into PCBM because of the mismatch between its work function and lowest unoccupied molecular orbital (LUMO) of PCBM. Figure 4a shows the experimental dark current densities (J_D) of the hole-only devices. This observation is common for disordered semiconductors with low mobility and can be used to directly determine the hole mobility of the PSCs approximately following the formulation 3[27]

$$J_h = \frac{9}{8}\varepsilon_0\varepsilon_r\mu_h \exp\left(0.891\gamma_h\sqrt{\frac{V}{L}}\right)\frac{V^2}{L^3} \quad (3)$$

where J_h is the hole current, μ_h the zero-field mobility of the holes, γ_h the field activation factor, ε_0 the permittivity of free space, ε_r the relative permittivity of the material, and L the thickness of the active layer. The experimental data were fitted using formulation 3 and the resulting hole mobility for devices with SRGs was about 1.8×10^{-9} m^2 V^{-1} s^{-1}, whereas the hole mobility of reference devices was around 1.2×10^{-9} m^2 V^{-1} s^{-1}. About a 50% increase in hole mobility can be attributed to the orientation effect of SRGs.

The electrical process in PSCs can also be studied from internal quantum efficiency (IQE) data.[28] IQE data show the efficiency of photons absorbed changed into electronics. As shown in Figure 4b, PSCs with SRG structure show about 10% increased IQE compared with the reference PSCs in the visible region. SRGs with stalactite structure in HIL and photoactive layer can increase the interface areas between electrode and photoactive layer to improve charge extraction effectively.

The J−V characteristics PCE and fill factors (FF) of all the PSCs are shown in Figure 5. All PSCs are fabricated without

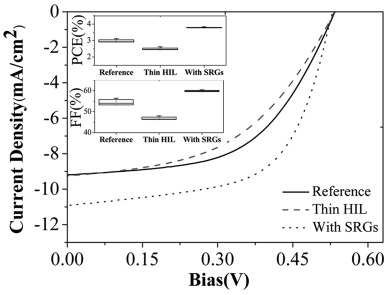

Figure 5. J−V characteristics of the different devices. Insert: PCE and FF of the different devices.

thermal annealing,[5,6] PCE of the reference PSCs is in the range of 2.9−3.0%. PSCs with SRGs present enhanced device performances, and an average PCE of 3.8% is obtained, which is roughly 27% increments compared with that of reference PSCs. The high FF (60%) shows little leakage current from stalactite structure in HIL. Although there were many large size pillarlike hills in HIL, but the active layer formed on HIL from solution by spin-coating would smooth hills. It is widely known that the details of SRG cannot be reproduced completely in film formation from solution; and there are no such big pillarlike hills in the active layer. Compared with reference PSCs, the similar R_{sh} and lower R_s of PSCs with SRGs confirms that rubbing method would not compromise the conductivity of HIL. The poorer performances of PSCs with the thinner HIL[29,30] further confirmed the enhancement of device performance resulting from the SRGs on the functional layers. Light trapping effect of the SRGs has a great contribution to the enhanced J_{sc} from 9.2 to 10.9 mA/cm^2, and the orientation effect of the SRGs leads to the higher FF from 0.55 to 0.60. Combined theory analysis with experimental data, it is demonstrated that SRGs in HIL, photoactive layer and cathode have three advantages in photovoltaic response: (1) effective light trapping induced by using an periodic grating without increasing photoactive layer thickness; (2) improved charge extraction through the increased interface area between electrode and the photoactive layer; (3) SRGs with stalactite structure in HIL lead the orientation of P3HT chains at certain degrees, which leads to a better carrier transport.

4. CONCLUSION

In conclusion, a simple rubbing method is used to fabricate PSCs with SRGs in HIL, photoactive layer and cathode, which show an average PCE of 3.8% with a 27% improvement compared with the reference PSCs. Different from the directly rubbing donor polymer leading to a high dichroic ratio, the PSCs built on the rubbed HIL show a lower dichroic ratio for the polarized light and higher absorption for sun light. Fortunately, SRGs with stalactite structure lead the orientation of P3HT chains and increase interface areas between electrode and photoactive layer, which contribute to a better electrical properties of PSCs. Due to the advantages in convenience and nondamage to photoactive layer, triplet SRGs formed by rubbing HIL will cast light on the realization of high-efficiency and low-cost PSCs.

AUTHOR INFORMATION

Corresponding Author

*E-mail: hongyuzhen@zju.edu.cn (H.Y. Zhen).

Notes

The authors declare no competing financial interest.

ACKNOWLEDGMENTS

This work was financially supported by the National Natural Science Foundation of China (61007056), Research Fund for the Doctoral Program of Higher Education of China (Grant 20100101120048).

REFERENCES

(1) Park, S. H.; Roy, A.; Beaupre, S.; Cho, S.; Coate, N.; Moon, J. S.; Moses, D.; Leclerc, M.; Lee, K.; Heeger, A. J. *Nat. Photon.* **2009**, *3*, 297−302.

(2) Chen, H. Y.; Hou, J. H.; Zhang, S. Q.; Liang, Y. Y.; Yang, G. W.; Yang, Y.; Yu, L. P.; Wu, Y.; Li, G. *Nat. Photon.* **2009**, *3*, 649−653.

(3) Liang, Y. Y.; Xu, Z.; Xia, J. B.; Tsai, S. T.; Wu, Y.; Li, G.; Ray, C.; Yu, L. *Adv. Funct. Mater.* **2010**, *22*, E135−E138.

(4) Kim, Y.; Shin, M.; Kim, H.; Ha, Y.; Ha, C. S. *J. Phys. D: Appl. Phys.* **2008**, *41*, 225101.

(5) Chen, H. Y.; Yang, H. C.; Yang, G. W.; Sista, S.; Zadoyan, R.; Li, G.; Yang, Y. *J. Phys. Chem. C.* **2009**, *113*, 7946.

(6) Peet., J. J.; Kim, J. Y.; Coates, N. E.; Ma, W. L.; Moses, D.; Heeger, A. J.; Bazan, G. C. *Nat. Mater.* **2007**, *6*, 497−500.

(7) Afre, R. A.; Hayashi, Y.; Soga, T. *J. Phys. D: Appl. Phys.* **2009**, *42*, 042002.

(8) Kim, J. Y.; Kim, S. H.; Lee, H. H.; Lee, K.; Ma, W.; Gong, X.; Heeger, A. J. *Adv. Mater.* **2006**, *18*, 572−576.

(9) Tumbleston, J. R.; Ko, D. H.; Samulski, E. T.; Lopez, R. *Appl. Phys. Lett.* **2009**, *94*, 043305.

(10) Lin, A.; Phillips, J. *Sol. Energy Mater. Sol. Cells* **2008**, *92*, 1689−1696.

(11) Emah, J. B.; Curry, R. J.; Silva, S. R. P. *Appl. Phys. Lett.* **2008**, *93*, 103301.
(12) Na, S. I.; Kim, S. S; Jo, J.; Oh, S. H.; Kim, J.; Kim, D. Y. *Adv. Funct. Mater.* **2008**, *18*, 3956−3963.
(13) Kim, M. S.; Kim, J. S.; Cho, J. C.; Shtein, M.; Guo, L. J.; Kim, J. *Appl. Phys. Lett.* **2007**, *90*, 123113.
(14) Kim, S. S.; Na, S. I.; Jo, J.; Kim, D. Y.; Nah, Y. C. *Appl. Phys. Lett.* **2008**, *93*, 073307.
(15) Lee, J. Y.; Connor, S. T.; Cui, Y.; Peumans, P. *Nano Lett.* **2008**, *8* (2), 689−692.
(16) Min, C. J; Li, J.; Veronis, G.; Lee, J. Y.; Fan, S. H.; Peumans, P. *Appl. Phys. Lett.* **2010**, *96*, 13302.
(17) Cocoyer, C.; Rocha, L.; Sicot, L.; Geffroy, B.; de Bettigines, R.; Sentein, C.; Fiorini-Debuisschert, C. *Appl. Phys. Lett.* **2006**, *88*, 133108.
(18) Hsiao, Y. S.; Chen, C. P.; Chao, C. H.; Wang, W. T. *Org. Electron.* **2009**, *10*, 551−561.
(19) Wang, D. H.; Choi, D. G.; Lee, K. J.; Jeong, J. H; Jeon, S. H.; O Park, O.; Park, J. H. *Org. Electron.* **2010**, *11*, 285−290.
(20) Zhen, H. Y.; Li, G. L.; Zhou, K. Y.; Liu, X. *Opt. Express* **2010**, *18*, 15784−15789.
(21) Zhu, D. X.; Zhen, H. Y.; Ye, H.; Liu, X. *Appl. Phys. Lett.* **2008**, *93*, 163309.
(22) Videlot, C.; Fichou, D. *Synth. Met.* **1999**, *102*, 885−888.
(23) Zhu, R.; Kumar, A.; Yang, Y. *Adv. Mater.* **2011**, *23*, 4193−4198.
(24) Zhu, D. X.; Zhen, H. Y.; Ye, H. *Acta Phys. Sin.* **2009**, *58*, 596−601.
(25) Zhu, D. X.; Shen, W. D.; Ye, H.; Liu, X.; Zhen, H. Y. *J. Phys. D: Appl. Phys.* **2008**, *41*, 235104.
(26) Gaylord, T. K.; Moharam, M. G. *Proc. IEEE* **1985**, *73* (5), 894−937.
(27) Mihailetchi, V. D.; Xie, H. X.; de Boer, B.; Koster, L. J. A.; Blom, P. W. M. *Adv. Funct. Mater.* **2006**, *16*, 699−708.
(28) Ko, D. H.; Tumbleston, J. R.; Zhang, L.; Williams, S.; DeSimone, J. M.; Lopez, R.; Samulski, E. T. *Nano Lett.* **2009**, *9*, 2742−2746.
(29) Lee, S. H.; Kim, J. H.; Shim, T. H.; Park, J. G. *Electron. Mater. Lett.* **2009**, *5* (1), 47−50.
(30) Kim, M. S.; Kim, B. G.; Kim, J. S. *ACS Appl. Mater. Interfaces* **2009**, *1* (6), 1264−1269.